



# Magnetic Fabric Analyses of Basin Inversion: A Sandbox Modelling Approach

Thorben Schöfisch<sup>1</sup>, Hemin Koyi<sup>1,2</sup>, Bjarne Almqvist<sup>1</sup>

<sup>1</sup>Hans Ramberg Tectonic Laboratory, Department of Earth Sciences, Uppsala University, Uppsala, 75236, Sweden

5 <sup>2</sup>Currently at: Department of Earth Sciences, Khalifa University of Science and Technology, Abu Dhabi, 127788, United Arab Emirates

*Correspondence to:* Thorben Schöfisch (thorben.schofisch@geo.uu.se)

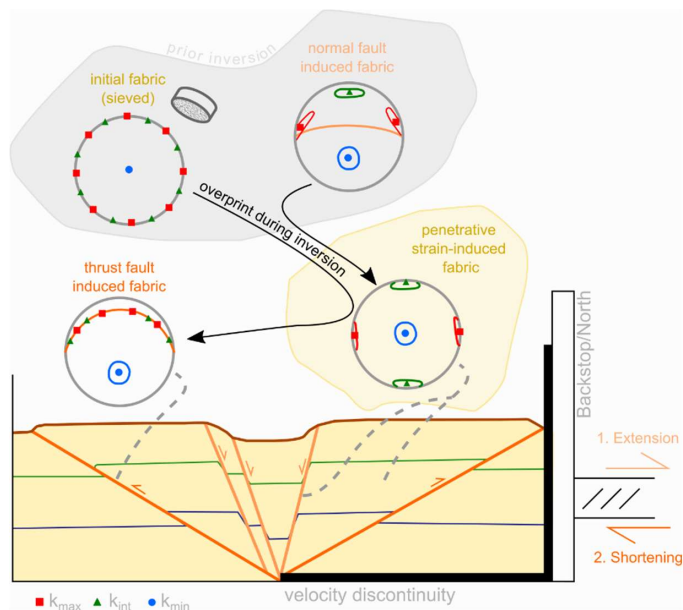
## Abstract.

Magnetic-fabric analysis is a useful tool to display deformation in nature and in models. In this study, three sandbox models  
10 represent basin inversion above a velocity discontinuity (base-plate). After complete deformation of each model, samples were  
taken in different parts of the models (along faults and areas away from faults) for magnetic fabric analysis. Model I, which  
simulates basin formation during extension, shows two kinds of magnetic fabric: an undeformed/initial fabric in areas away  
from faults, and a normal fault-induced fabric with a magnetic foliation that tends to align with the fault surface. Models II  
and III, which were initially extended before they were shortened, developed thrust faults during inversion. The thrusts show  
15 an alignment of magnetic foliation parallel to the fault surfaces that depends on the maturity of the thrust. Our results highlight  
that thrusting is more efficient in aligning the magnetic fabric along them compared to normal faults. Moreover, models II and  
III reveal a magnetic fabric overprint towards a penetrative strain-induced fabric (magnetic lineation perpendicular to  
shortening direction) in areas away from thrust faults. Such overprint shows a gradual transition of a magnetic fabric to a  
penetrative strain-induced fabric and further towards a thrust-induced fabric during shortening/inversion. In contrast, extension  
20 (Model I) developed distinct magnetic fabrics without gradual overprint. In addition, pre-existing normal faults are also  
overprinted to a penetrative strain-induced fabric during model inversion. They define weak zones within the main pop-up  
imbricate and steepen during model inversion. Steepening influences the magnetic fabric at the faults, and, in general, the  
strain propagation through the model during inversion.

The magnetic fabric extracted from the models presented here reflect the different stages of basin development and inversion.  
25 This study is a first attempt of applying magnetic-fabric analyses on models simulating inverted basins. However, the outcome  
of this study illustrates the possibility of applying a robust tool, i.e., magnetic-fabric analyses, to sandbox models, whose initial,  
intermediate, and final stages are well documented.



### 30 Graphical Abstract.





## 1 Introduction

Anisotropy of magnetic susceptibility (AMS or magnetic fabric) is a useful strain indicator in analogue models simulating compressional tectonic regimes (Almqvist and Koyi, 2018; Schöfisch et al., 2020; Schöfisch et al., 2022). AMS measurements provide information about the bulk orientation of the magnetized grains within a collected sample. From the AMS measurements, a magnetic susceptibility ellipsoid with three principal axes of susceptibility ( $k_{\max} \geq k_{\text{int}} \geq k_{\min}$ ) is described. Analyses of the susceptibility ellipsoid is similar to the strain ellipsoid, and changes of the magnetic ellipsoid can be related to strain changes (e.g., Hrouda and Janák, 1976; Jelinek, 1981; Kligfield et al., 1981; Hrouda, 1982; Hirt et al., 1988; Borradaile 1988, 1991; Borradaile and Henry, 1997; Bakhtari et al., 1998; Parés, 1999; Parés and van der Pluijm, 2002; Borradaile and Jackson, 2004; Burmeister et al., 2009; Parés, 2015).

Several publications summarize the magnetic fabric development of basin and its inversion derived from analyses of natural examples (e.g., Sagnotti et al., 1994; Mattei et al., 1997, 1999; Cifelli et al., 2005; Soto et al., 2007, 2008, 2012, 2016; Oliva-Urcia et al., 2010, 2013, 2016; García-Lasanta et al., 2014, 2015, 2018; Marcén et al., 2019; Burgin et al., 2021). Relating the magnetic fabric observed in extensional settings reveals an overprint of a sedimentary fabric by an extension-related fabric, which shows a magnetic lineation ( $k_{\max}$  axes clustering) parallel to extension. With the development of normal faults, the magnetic lineation develops parallel to the transport direction (i.e., a shear-related fabric) along the fault surface (Marcén et al., 2019) or perpendicular to the faults (Cifelli et al., 2005). Extensional magnetic fabrics can be preserved during basin inversion when either shortening is not significant enough or thrust development accommodates shortening and a passive displacement of the basin prevents overprinting of the magnetic fabric. Where magnetic fabric is overprinted during inversion, the development of the magnetic fabric depends on the inversion style (García-Lasanta et al., 2018). According to observations by Averbuch et al. (1992), Bakhtari et al. (1998), Parés et al. (1999), and Parés and van der Pluijm (2002), the magnetic fabric (i.e., magnetic foliation defined by a girdle distribution of  $k_{\max}$  and  $k_{\text{int}}$  axes) becomes parallel to the developed tectonic foliation. Also, a magnetic lineation develops parallel to an intersection lineation that later changes into a stretching lineation with increasing deformation.

The effect of overprinting of an existing “sedimentary” magnetic fabric by a tectonic fabric is supported by results of analogue sandbox models (Almqvist and Koyi, 2018; Schöfisch et al., 2020; Schöfisch et al., 2022). Even though the effects of grain deformation, fluidal movement or recrystallization (i.e., changes in magnetic mineralogy and development of sub-fabric) on magnetic fabric development are not represented in sandbox models simulating upper crustal deformation, analogue modelling highlights the importance of grain reorientation during deformation (e.g., Schöfisch et al., 2022). This study evaluates the potential of AMS as a strain gauge in sandbox models simulating the development of basin and basin inversion. Furthermore, this study aims to understand the development of magnetic fabric in extensional settings and its overprint during basin inversion.



## 2 Methods

### 2.1 Experimental Setup

#### 2.1.1 Model Preparation

For this study, three models (I, II, III) were prepared with a similar base plate setup (Fig. 1) at room temperature (22°C and humidity of 50-60%). Models were initially 8.3 cm thick, 30 cm wide and 40 cm long. A basal metal plate was attached to the moveable backstop that created a velocity discontinuity in the middle of model (20 cm from the backstop) beneath the layers of sand-magnetite mixture (Fig. 1). The sand-magnetite mixture was used to simulate the brittle behaviour of sedimentary rocks in the upper crust and consist of loose sand and magnetite (< 0.1 vol%), both with similar subangular shape and grain size (0.124-0.356 mm). The artificial high content of ferromagnetic magnetite in the models (compared to natural examples) governs the bulk signal of the AMS and the influence of the diamagnetic sand can effectively be neglected. Single layers of sand-magnetite mixture were carefully sieved from a height ranging between 30-50 cm above the model. The layers, which had varying thickness (0.9-1.5 cm) due to sieving by hand, were separated by a thin layer of coloured sand acting as passive marker. The rationale behind sieving the sand-magnetite into the sandbox and accepting irregularities in layer thickness throughout the model was to avoid scraping, which creates an artificial magnetic lineation as an initial magnetic fabric (e.g., Schöffisch et al., 2022). The uppermost layer of each model consisted of sand only and was scraped after sieving to create an even model surface with same model height for all three models. Note that this uppermost layer was not used in the AMS analysis. On the surface of the model, coffee powder was sieved as well as point markers (coloured sand) were set for monitoring surface deformation.

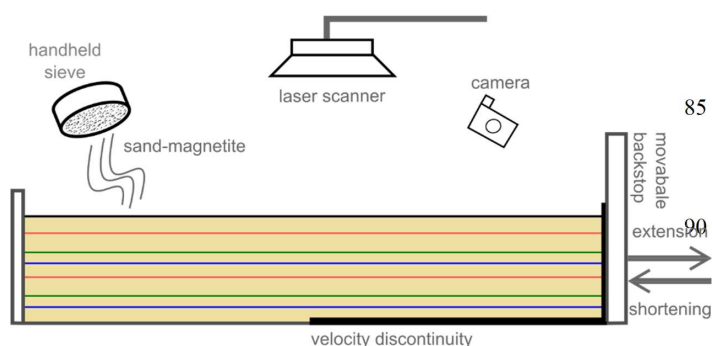


**Figure 1: Sketch of model setup.** Sieved layers of sand-magnetite are separated by coloured sand layers. A basal metal plate was used as velocity discontinuity and attached to the backstop that moved backwards for extension and forwards for shortening the model. The models were monitored by taking pictures from different angles with camera and model surfaces were monitored by laser scanning during deformation.

#### 2.1.2 Model Run, Sectioning, and Sampling

All three models (I, II, III), which were identical in setup, were extended up to 1 cm in total. However, only models II and III were inverted. During extension, the model runs were paused after 0.5 cm of extension to fill the developed basin. After the extension phase, models II and III were shortened by different amounts of bulk shortening to simulate basin inversion at different stages. Extension and shortening of the models were initiated by a constant moving backstop with a velocity of 3



cm/hr, to which a velocity discontinuity was attached. Model I simulated extension only. Model II was shortened by 1.5 cm after extension and stopped when first kinks developed (i.e., when sand layers were offset by millimetres), before any thrust fault forms with larger displacement. Model III was shortened by 4 cm after the initial 1 cm extension. This 4 cm amount of shortening represents the stage, when the backthrust of Model III showed a similar amount of displacement as the pre-existing normal fault. Moreover, the differences in the amount of bulk shortening between the models II and III allows a comparison of i) magnetic fabric of inverted basins with that of extensional stage, i.e., prior to shortening, ii) basin development and inversion with same amount of bulk extension and shortening, and iii) magnetic fabric at normal faults and thrust faults with similar displacement.

During deformation, the models were monitored by a series of photos from all sites. After final stage of deformation, models were carefully wetted for vertical sectioning parallel to the extension and shortening direction, as well as for allowing model sampling for AMS analysis. During the sampling, oriented plastic cubes (internal volume 1.7 cm<sup>3</sup>) were carefully pressed horizontally into the model. Each section was 2-2.5 cm wide. Before sampling a section, the next section was cut and a stable plate was placed between the two sections to support sampling of the outer section (i.e., pressing the cube into the cohesive sand-magnetite with stable support from the other side without exerting pressure on the next section). The cohesive and wetted AMS samples were stored in semidry conditions (fridge with 7°C and humidity of 75%), allowing for AMS measurements over a few weeks before the material inside the plastic cube loses its cohesion.

In total, 721 samples (Model I: 217, Model II: 241, Model III: 263) were taken across the models targeting the different structures. The focus of sampling was to acquire magnetic fabrics of different parts of the models (e.g., normal faults, thrusts, graben, footwalls, hangingwall-imbricates). This exercise eliminated the effect of measuring a bulk mixed AMS fabric, which may be created due to a small structure-to-sample-size ratio. However, it is not possible to entirely diminish this effect at faults. Sampling at faults covers the narrow fault zone and the vicinity of a fault. The vicinity of a fault might have a different magnetic fabric than observed directly at a fault plane. Consequently, a mixed fabric is represented by the bulk measurement of samples from fault zones. Such an effect needs to be considered during magnetic fabric interpretation of fault-associated datasets. Therefore, a structure-to-sample-size ratio is calculated (see Fig. S1 in Supplementary Material).

### 2.1.3 AMS Measurement and Analysis

The bulk susceptibility and magnitude of AMS samples was measured with a MFK1-FA Kappabridge (Agico Inc.) in a low-field (976 Hz) with an AC field strength of 200 A/m at room temperature. The grains within a sample respond to an applied external magnetic field, and the directional variation of the “response” (magnetic susceptibility) is described through a symmetric second-rank tensor with six independent matrix elements. The eigenvalues and eigenvectors of the matrix are the principal axes of susceptibility ( $k_{\max} \geq k_{\text{int}} \geq k_{\min}$ ) that describe the magnitude, orientation, and shape of a magnetic susceptibility ellipsoid. The maximum axis ( $k_{\max}$ ) describes the magnetic lineation, whereas the plane containing the maximum and intermediate axes ( $k_{\max}$  and  $k_{\text{int}}$ ) describe the magnetic foliation. Orientation of the principal axes were plotted in an equal-area lower hemisphere projections with north assigned towards the backstop of the model. The corrected degree of anisotropy



( $P_j = \exp\sqrt{2(n_{\max} - n_{\text{mean}})^2 + (n_{\text{int}} - n_{\text{mean}})^2 + (n_{\min} - n_{\text{mean}})^2}$ ), with  $n_{\max} = \ln(k_{\max})$ ,  $n_{\text{int}} = \ln(k_{\text{int}})$ , and  $n_{\min} = \ln(k_{\min})$ ) reveals information about the sorting of grains within a sample, where a high degree of anisotropy corresponds to a preferred alignment of grains, whereas a low degree of anisotropy indicates a variation of grain orientations (Hrouda, 1982). Additionally, the shape of the susceptibility ellipsoid is described by  $T = [2n_{\text{int}} - n_{\max} - n_{\min}] / [n_{\max} - n_{\min}]$ , where  $T = 1$  represents an oblate shape,  $T = 0$  is neutral triaxial shape, and  $T = -1$  is a rotational prolate shape. The principal axes, the corrected degree of anisotropy ( $P_j$ ), or the shape of anisotropy ( $T$ ) were statistically interpreted and visualized with the help of graphical tools, MATLAB, and ArcGIS. The centre of each AMS sample defined the distance to a fault or the model surface (i.e., depth). Samples that were not perfectly located with their centres on a fault were still assigned to the fault-induced AMS dataset. Therefore, we introduced a threshold with a range of 0.8 cm (centre to corner of a sample) between their centre to a fault. Samples located within this threshold were labelled to be fault-induced. Furthermore, in section view, the area of a sample was compared to the area of the fault zone, and a sample-size-to-structure ratio is calculated (Fig. S1 in Supplementary Material). This ratio allows specifying the amount of AMS signal induced by a fault relative to that induced by the non-faulted area within the sample. Note that interpretations of the magnetic fabric within the grabens are limited to the small number of samples and no solid statistical interpretation can be taken for internal graben changes.

### 3 Results

#### 3.1 Model I: Basin formation (extension only)

Model I developed an east-west striking graben structure bounded by two normal faults that dip 60-70° towards each other (Fig. 2). The south-dipping normal fault (northern fault/Normal Fault B) shows a displacement of ~1.4 cm. With progressive extension, a couple of synthetic and antithetic faults form in the hanging-wall of the graben (Fig. 2). AMS analysis of different parts of this model reveals that there is no sign of deformation in the footwalls on either side of the graben; it shows the oblate initial fabric that is produced by sieving, with  $k_{\min}$  axes clustering vertical, as the pole of bedding, and  $k_{\text{int}}$  and  $k_{\max}$  axes spread in the horizontal plane along a primitive circle (Fig. 2). The magnetic fabric in Footwall B is more scattered and has a lower degree of anisotropy compared to the magnetic fabric in Footwall A. Within the graben, the magnetic fabric is similar to the fabric observed in the footwalls and shows the initial fabric (Fig. 2). However, the magnetic fabric along the normal faults differ from the initial fabric as  $k_{\min}$  axis is rotated away from its vertical orientation, and  $k_{\max}$  and  $k_{\text{int}}$  axes have formed a subhorizontal (10-20°) magnetic foliation (Fig. 2). The rotation direction of  $k_{\min}$  axis is determined by the dip direction of the normal fault; the  $k_{\min}$  axis rotated in the opposite direction of the fault dip. However, generally, there is a tendency of the magnetic foliation to align parallel to the fault surface (Fig. 2). Moreover, the fabric is mostly oblate, but the degree of anisotropy is lower along the normal fault compared to the fabric in the graben (hanging wall) and its footwalls (Fig. 3a, and d).

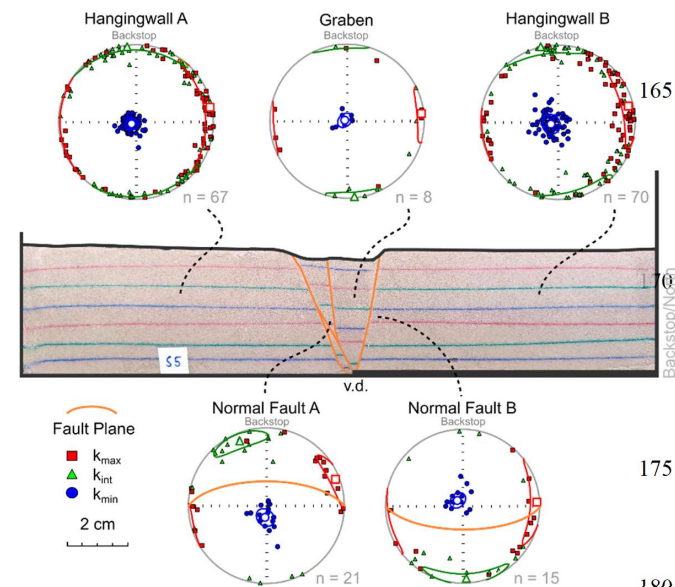


Figure 2: Model I shows a graben that is bounded by normal faults (orange lines). The magnetic fabric for each structure/area is plotted on equal-area lower hemisphere projections with the confidence ellipses and mean of each principal axis.

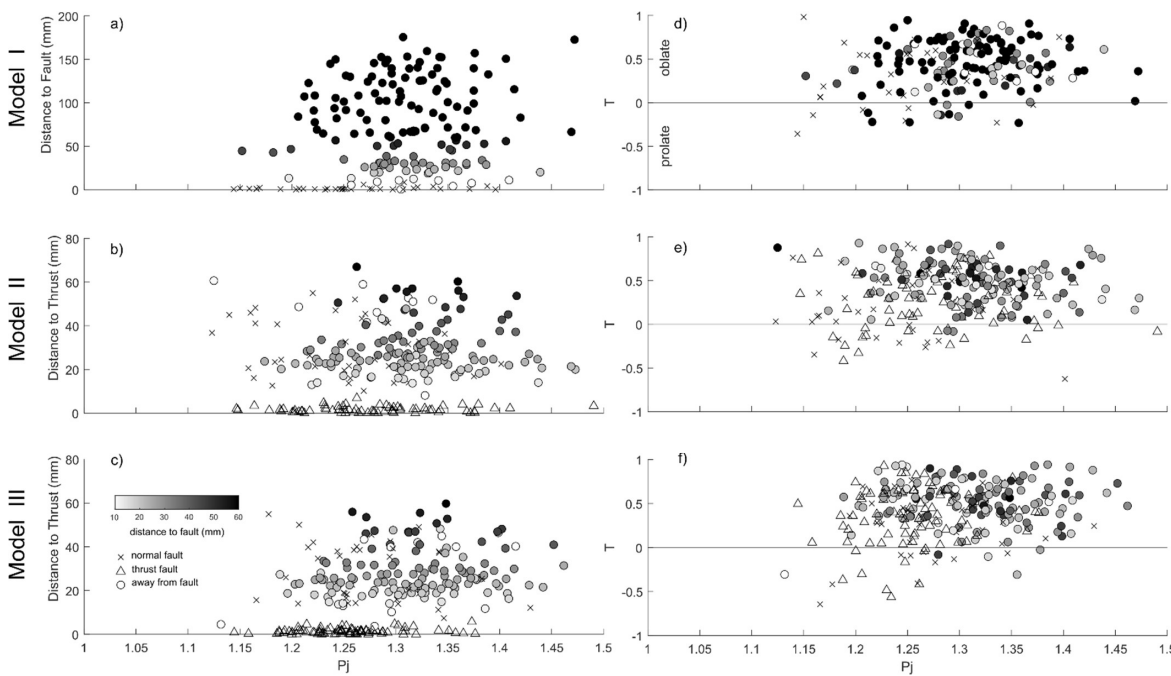


Figure 3: Distribution of degree of anisotropy ( $P_j$ ) is plotted against the distance to the closest fault/thrust (a,b,c) and against the shape of anisotropy ( $T$ ) (d,e,f) for each model. Note, the colormap of (a,b,c) is defined by the distance towards the closest normal fault, whereas the colormap of (d,e,f) is defined by the distance to the closest thrust fault.





### 3.2 Model II: Basin Inversion

The second model (Model II) was extended 1 cm and later shortened 1.5 cm. Similar to Model I, an east-west striking graben developed during extension (Fig. 4). With the onset of subsequent shortening of the model, the normal faults steepened by  $\sim 2-3^\circ$ , which led to a slight narrowing of the graben (Fig. S1 in Supplementary). The dip of the faults is steeper ( $70-85^\circ$ ) than that of the normal faults of Model I. However, the normal faults did not display any significant reactivation, during the subsequent shortening. Instead, precursors of gently-dipping thrust faults ( $25-35^\circ$ ) developed as kinks, which offset footwall markers by a few millimetres. These “thrust faults” are less mature than the normal faults as they developed less displacement. The magnetic fabrics of footwalls A and B, as well as of the hangingwall-imbricates A and B show an oblate magnetic fabric that is similar to the initial fabric (vertical  $k_{\min}$  axis, and horizontal spread of  $k_{\max}$  and  $k_{\text{int}}$  axes) (Fig. 4). Furthermore, there is no clear distinction between the degree of anisotropy between the footwall and hanging wall areas. Additionally, the central graben reveals similar magnetic fabric as those in footwalls and hangingwall-imbricates (Fig. 4). The magnetic fabrics at the normal faults A and B display a scatter of subvertical  $k_{\min}$  axes. The mean of the subvertical  $k_{\min}$  axes points steeply to the south for Normal Faults A and to the north for Normal Fault B. The  $k_{\max}$  and  $k_{\text{int}}$  axes are mostly oriented subhorizontally ( $< 30^\circ$ ) with a dominant east-west orientation for  $k_{\max}$  axes and north-south for  $k_{\text{int}}$  axes (Fig. 4). Magnetic foliation along the normal fault surface is less pronounced than that along the normal faults in Model I. AMS data from the thrust faults in Model II show a similar principal axes distribution as the normal faults (Fig. 4). However, the  $k_{\max}$  and  $k_{\text{int}}$  axes for each thrust fault tend to define a magnetic foliation subparallel to the thrust faults. In Model II, the magnetic fabric along both the normal faults and the thrust faults is mainly oblate with some occurrences of prolate shape (Fig. 3). The degree of anisotropy is comparable between the normal and thrust faults, but it is on average lower than in areas away from the faults (Fig. 3).

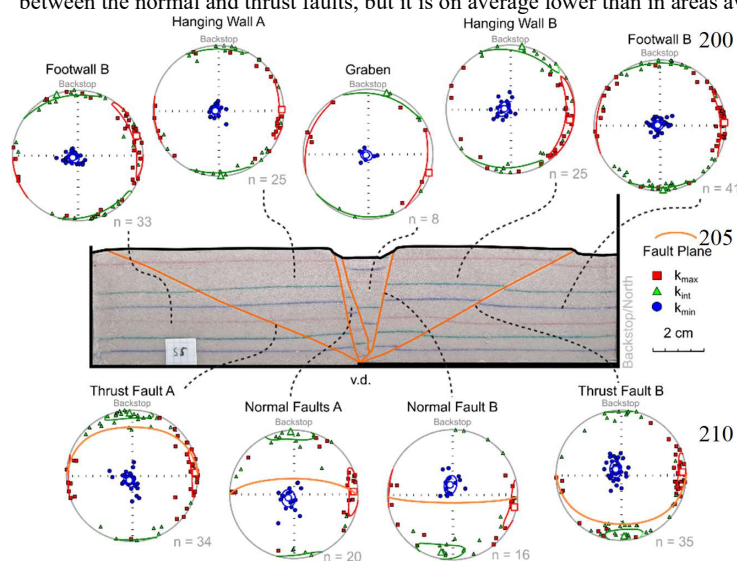


Figure 4: Model II with its developed structures. The associated magnetic fabric of each structure/area are plotted on equal-area lower hemisphere projections with confidence ellipses and mean of each principal axis.





### 215 3.3 Model III: Inverted Basin Model (advanced shortening)

Model III shows similar structures to those in Model II. However, the thrust faults in Model III, which was subjected to larger amount of bulk shortening (+3 cm), are more mature and display larger displacement than those in Model II (Fig. 5). The normal faults dip 70-80° and show a displacement of ~1.4 cm in average. During inversion, Normal Fault B steepened by ~5°, whereas Normal Faults A remain with the dip that is observed prior to shortening (Fig. S1 in Supplementary). Similar to Model

220 II, with subsequent shortening, the pre-existing graben narrowed with rotation of the normal faults by few degrees (Fig. S1 in Supplementary). The thrust faults dip in a range between 25-40° and show displacement of ~1.4 cm similar to that along the normal faults. Additionally, the southern thrusts (i.e., Thrust Fault A) splays in the deeper parts of the model (Fig. 5).

In Model III, the magnetic fabric in footwalls A and B, the hangingwall-imbricates A and B, and the graben are similar to the initial fabric, which is also similar to the magnetic fabrics from equivalent areas of the other two models. In Footwall B,  $k_{\max}$  axes are clustering horizontally along east or west directions instead of spreading around the primitive circle. Furthermore,  $k_{\text{int}}$  axes also cluster mainly in a north and/or south direction. Clustering of  $k_{\max}$  and  $k_{\text{int}}$  axes in the Footwall B is different from that in Footwall A, graben, and hangingwall-imbricates, where  $k_{\max}$  and  $k_{\text{int}}$  axes are spread around the primitive circle. (Fig. 5). The principal axes ( $k_{\max}$ ,  $k_{\text{int}}$ , and  $k_{\min}$  axes) distribution along the normal faults in Model III is comparable to that along the normal faults of Model II (Fig. 5). The cluster of  $k_{\min}$  axes (i.e., mean of  $k_{\min}$  axes orientations) rotates slightly away from

230 its vertical orientation to subvertical orientation, dipping south for the Normal Faults A and dipping north for the Normal Fault B.

AMS analysis does not show a clear girdle distribution of  $k_{\max}$  and  $k_{\text{int}}$  axes parallel to the normal fault surface (Fig. 5). However,  $k_{\max}$  axes cluster horizontally towards the East or West (i.e., perpendicular to the extension and shortening directions), whereas  $k_{\text{int}}$  axes distribute along a North to South axis (i.e., parallel to extension and shortening directions).

235 Nevertheless, along Normal Fault A, the magnetic foliation tends to be sub-parallel to the fault surface (Fig. 5). In contrast, the magnetic foliation is parallel to the thrust fault in Model III. Even though displacement along the thrust faults is comparable to that along the normal faults of the model, the magnetic foliation associated with thrusting is distinct (*cf.* Schöfisch et al., 2022). The degree of anisotropy of the normal faults is similar to that of the thrust faults with similar distribution of the shape of anisotropy, which mainly plots in the oblate field with some degree of prolate signature. The degree and shape of anisotropy

240 along the structures in Model III are similar to that in the other two models (Fig. 3).

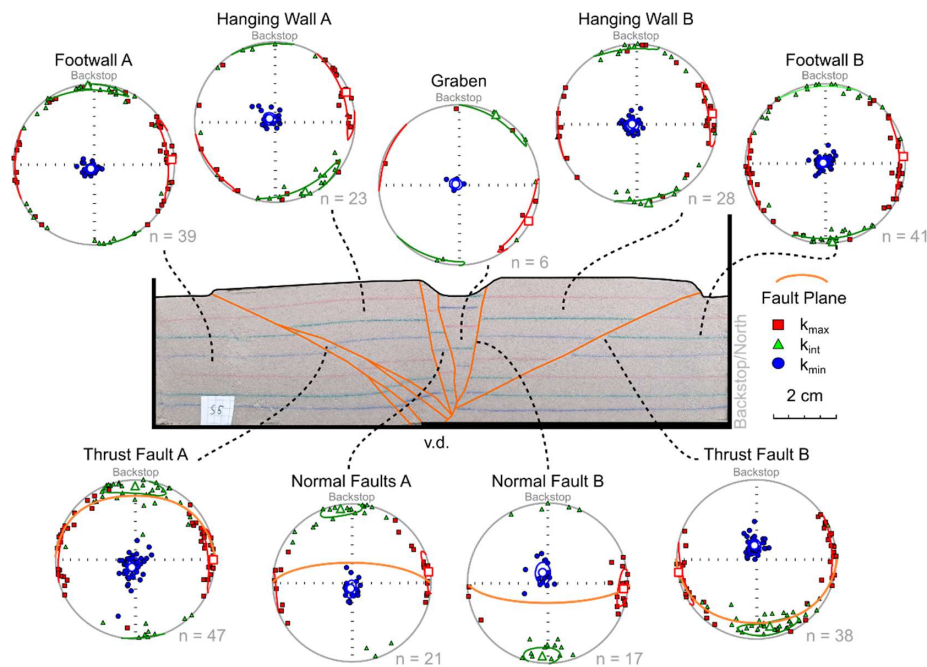


**Figure 5: Model III with its developed structures. The associated magnetic fabric of each structure/area are plotted on equal-area lower hemisphere projections with confidence ellipses and mean of each principal axis.**

## 245 4 Discussion

### 4.1 Initial magnetic fabric

The initial fabric of the models was created by sieving, where  $k_{min}$  axes cluster as the pole to bedding, and  $k_{max}$  and  $k_{int}$  axes orient randomly in the horizontal plane parallel to bedding. This initial fabric is the reference and changes from this initial fabric are attributed to deformation. Sieving the initial magnetic fabric is a novelty, tested in this study, and introduced in  
 250 sandbox models simulating compressional tectonic regimes (Schöfisch et al., in prep). The sieved fabric differs from the scraped fabric; a scraped initial fabric shows horizontal alignments of  $k_{max}$  axes parallel and  $k_{int}$  perpendicular to the scraping direction (Almqvist and Koyi, 2018, Schöfisch et al., 2020; 2022), whereas  $k_{max}$  and  $k_{int}$  axes in a sieved magnetic fabric distribute randomly in different horizontal directions. Such a sieved magnetic fabric is similar to a sedimentary fabric that is observed in nature (cf. Borradaile and Henry, 1997; Bakhtari et al., 1998; Parés et al., 1999) and allows an improved  
 255 interpretation and comparison between models and natural analogies (Schöfisch et al., in prep).

The footwalls A and B of Model I are undeformed and reveal still the initial fabric after extension. It can be noted that the magnetic fabric in Footwall B of Model I has a relatively larger scatter compared to Footwall A of the same model. Footwall



B is resting on the basal plate and we assume that the deviation in magnetic fabric is due to grain reorientation/bulk compaction of sand due to vibration during movement of the underlying plate. Models II and III also retain the initial fabric in some locations even after model inversion. Consequently, these locations with initial fabric in models II and III indicate undeformed areas. Such undeformed areas during basin development are also known from natural examples (Olivia-Urcia et al., 2013; Garcia Lasanta 2018).

## 4.2 Extensional fabric in basin model

In a natural sedimentary basin, a magnetic lineation (i.e.,  $k_{\max}$  clustering) develops parallel to the axis of extension. This observation derives from studying the reorientation of phyllosilicates in clay-rich sediments (e.g.; Mattei et al., 1997; 1999; Cifelli et al., 2005). However, the surface markers of the models of this study indicate movement of the individual developed hanging- and footwall (i.e., graben and Footwall B) without noticeable internal deformation (i.e., stretching) of the lithology during extension of the models. The magnetic fabric within the hanging- and footwall of Model I has not developed a clear magnetic lineation parallel to stretching and rather indicates localized deformation, where the normal faults are developed. Consequently, our results underscore that there is minimal to no layer-parallel deformation/extension within the different hanging- and footwalls during extension in such brittle deformation environment (i.e., using a ridged velocity discontinuity/basal plate for initiating deformation).

The normal faults of Model I show a magnetic foliation that vaguely align parallel to the fault surface. However, this alignment is very weak and there is a large difference of  $\sim 50^\circ$  between the inclinations of magnetic foliation and of the fault surface (Fig. 2). Nevertheless, the magnetic fabric of the normal faults differs to the initial fabric, especially, the degree of anisotropy is generally lower at normal faults compared to the rest of the model, which mainly show the initial fabric. These differences in magnetic fabric in Model I are results of extensional deformation. Although, there is no presence of a layer-parallel extensional fabric, an “extensional fault-induced fabric” (i.e., normal fault-induced fabric) developed in Model I as consequence of localized deformation during basin development.

## 4.3 Overprint of magnetic fabric in models during inversion

### 4.3.1 Thrust overprint

Models II and III simulate basin inversion at different stages. Model II developed kinks along the thrust surfaces that offset the layers by a few millimetres, whereas Model III developed more mature thrusts that offset the layers in the model by the same amount as the pre-existing normal faults (Figs. 4, and 5). It has been reported that compaction and folding (i.e., kinking) takes place prior to thrusting (e.g., Mulugeta and Koyi, 1992; Koyi, 1995; Koyi et al., 2003). The different thrusts in the models follow the same deformation path and reveal a magnetic fabric that is associated with their development. Model I shows an



290 initial fabric at the same location/area where the thrusts developed in models II and III. Therefore, the development of the thrust-induced fabric in the models of this study follow a similar evolution of fabric development (from initial fabric via a penetrative strain-induced fabric towards the thrust-induced fabric) as observed in a recent study by Schöfisch et al. (2022). Moreover, Schöfisch et al. (2022) related the alignment of magnetic foliation parallel to the thrust surface with maturity of a thrust. Similar observations are made in the current models; magnetic foliation shows a closer alignment with thrusts of Model  
 295 III than with the thrust surfaces (i.e., kinks) in Model II.

The overprint of magnetic fabric during thrusting differs to/from the overprint observed at the normal faults. The alignment of fabric to the thrust surfaces is displayed by  $k_{\max}$  and  $k_{\text{int}}$  axes defining a broad girdle distribution (i.e., magnetic foliation) parallel to the thrust surface. The normal faults show also a broad scatter (referring to Model I, whereas normal faults in models  
 300 II and III show an additional overprint during inversion; discussed in section 4.3.2). The broad scatter in this girdle distribution seems to be an artefact of sampling and the related structure-to-sample-size ratio (Fig. S2 in Supplementary). However, such artefact cannot be the reason for a large discrepancy between magnetic foliation and fault geometry at the normal faults in the models. Comparing the magnetic fabric from the normal faults to the thrusts, with the similar displacement along the fault surface (Figs.2, 3, and 4), it is apparent that thrusting is more efficient in aligning grains parallel to a fault.

305

#### 4.3.2 Magnetic fabric overprint at normal faults

Normal faults of the models II and III show no or very minor reactivation during inversion, which is in agreement with observations of pure-dry-sand models by Eisenstadt and Sims (2005) and Deng et al. (2019). However, the grabens of models II and III become narrower during inversion and the normal faults rotate slightly to steeper angles (Fig. S1 in Supplementary).  
 310 Such basin narrowing and fault rotation are consequences of the development of the main pop-up imbricate that is bounded by the thrusts in models II and III. As compaction precedes thrusting, the sand package, including the graben and normal faults, experiences layer-parallel shortening. Similar to what has been reported in previous studies (cf. Eisenstadt and Withjack, 1995; Bonini et al., 2012), this layer-parallel shortening reworks the pre-existing extensional structures and the associated grain alignment. The magnetic fabrics at the normal faults of model II and III are rearranged from a normal fault-induced fabric  
 315 towards a penetrative strain-induced fabric during subsequent inversion/shortening of the models. In more detail, the normal faults of models II and III show a clustering of  $k_{\max}$  axes to the East and the West, and of  $k_{\text{int}}$  axes to the North and the South (Figs. 4, and 5). The clustering of  $k_{\max}$  and  $k_{\text{int}}$  axes is classified as penetrative strain-induced fabric that becomes more distinct with higher bulk shortening (comparing the normal faults in models II and III). This clustering in magnetic fabric differs from the  $k_{\max}$  and  $k_{\text{int}}$  axes distribution with elongated confidence ellipses of the normal faults in Model I. In conclusion, the normal  
 320 faults are less reactivated in the sense of kinematics, but rather show an overprint towards a penetrative strain-induced fabric accompanied by geometrical change of the fault with subsequent inversion.



### 4.3.3 Penetrative strain distribution during inversion

With the onset of model shortening (i.e., inversion), the models II and III were compacted before the thrusts developed. The models accommodated the penetrative strain by grain rearrangement, which is reflected by the change in magnetic fabric. Early signs of basin inversion in nature have been reported to be recognized by the reorientation and development of magnetic lineation perpendicular to shortening direction in a basin (e.g., De Lamotte et al., 2002; Soto et al., 2016). Such development of magnetic lineation perpendicular to shortening direction can be observed in the models II and III;  $k_{\max}$  axes cluster horizontally along an east-west axis (penetrative strain-induced fabric) in the areas away from the thrusts (Figs. 4, and 5). However, depicting deviations of the initial fabric in the models and referring this to penetrative strain, especially, when rotation and clustering of a magnetic lineation are parallel to bedding, needs careful interpretation. Some  $k_{\max}$  orientations differ from the penetrative strain-induced fabric within the footwalls and hanging wall-imbricates of the models. This means a mixture is monitored between a penetrative strain-induced fabric ( $k_{\max}$  cluster perpendicular to the shortening direction) and the initial fabric ( $k_{\max}$  axes spread around the primitive circle) in these areas away from thrusts (Figs. 4, and 5). It is common that the initial fabric prevails in some locations even after basin inversion in nature (Olivia-Urcia et al., 2013) and in sandbox models (Schöffisch et al., 2022). An observation of a mixture between initial fabric and penetrative strain-induced fabric, or a prevailing initial fabric after deformation, indicates that penetrative strain is heterogeneously distributed within the model and further, imbricates deform internally heterogeneously.

Heterogenous penetration of strain within the model occur due to accommodation of strain during inversion by pre-existing structures like normal faults (cf. Eisenstadt and Withjack, 1995; Bonini et al., 2012, Tong et al. 2014). The pre-existing normal faults create weak zones within the main pop-up structure, which develops during inversion. These weak zones accommodate most of the penetrative strain within the pop-up imbricate during model inversion and therefore, deform internally, as seen by the geometric reorientation of the normal faults. Normal faults in models II and III develop a magnetic lineation during inversion that is similar to the magnetic fabric induced by layer-parallel shortening ( $k_{\max}$  axes cluster perpendicular to shortening direction) (see discussion 4.3.2). Consequently, the normal faults accommodate strain, and the geometric change of the normal faults are signs of internal, penetrative deformation within a pop-up imbricate during inversion. Such accommodation of strain by pre-existing faults contribute to a heterogenous internal deformation that results in a mixed magnetic fabric within both the footwall and hanging walls.

350



#### 4.3.4 Gradient in magnetic fabric with increasing bulk shortening

Shortening in the models is driven by the backstop and the velocity discontinuity from one direction (i.e., from the model North). Therefore, areas closer to the backstop and velocity discontinuity compact before deformation penetrates farther into the model (Mulugeta and Koyi, 1992; Koyi, 1995). This is seen by a clear and distinct magnetic lineation (i.e., a penetrative strain-induced fabric) in Footwall B of Model III, which is the footwall next to the backstop. Areas farther from the backstop (e.g., Footwall A and hanging-wall imbricates of Model III) are also affected by penetrative strain, but, show a mixture between a penetrative strain-induced fabric and the initial fabric (as discussed earlier in 4.3.3). Consequently, it could be argued that there is a general gradient in amount of penetrative strain from modelling north to modelling south in the inverted models. However, such general gradient is not linear, because strain is also increasing with decreasing distance towards a thrust within thrust imbricates (Fig. 3) (cf. Schöfisch et al., 2022).

The magnetic fabric changes with increasing strain (e.g., Borradaile and Henry, 1997; Bakhtari et al., 1998; Parés et al., 1999), and analysing the degree of anisotropy is a useful approach to illustrate changes in magnetic fabric in analogue models (Almqvist and Koyi, 2018; Schöfisch et al., 2020, 2022). For example, a decrease in degree of anisotropy with decreasing distance to a fault, is observed (cf. Schöfisch et al., 2022). Generally, AMS data from faults in shortened models show a lower degree of anisotropy compared to the data from areas away from faults. This is also the case in extensional setting, e.g., in Model I, where AMS data from the normal faults highlight this observation, but it is apparent that the change in degree of anisotropy is abrupt between normal faults and farther away from the faults (Fig. 5). As discussed above (section 4.1), there is almost no penetrative strain developing within the footwall and hanging wall during extension. Normal faults develop from the onset of model extension (V1-2 in Supplementary Material S1), illustrating a distinct difference between magnetic fabric away from faults and within/along faults. In contrast, in compressional regime, penetrative strain (and kinking) precedes thrusting, which needs more amount of model shortening before a thrust fault is created, compared to the “amount” of model extension that is needed for formation of a normal fault (V1-2 in Supplementary Material S1). Penetrative strain is an important factor in changing the magnetic fabric and describes the transition of changes in magnetic fabric between the initial fabric to a thrust-induced fabric. In summary, unlike models II and III which show a transition in degree of anisotropy, Model I developed no gradual change in degree of anisotropy with distance to a thrust (Fig. 3). In addition, comparing model II and III, the gradient in degree of anisotropy becomes clearer with increasing bulk shortening, which is a similar observation as by Schöfisch et al. (2022). The decreasing gradient in the degree of anisotropy and, in general, the change in magnetic fabric with distance to faults are distinct features that describe the difference between extensional and compressional tectonic regimes.



## 5 Advantages, limitations, and future perspectives of applying AMS to basin and basin inversion models

### 5.1 Depicting deformation and changes in deformation by AMS

Applying AMS allows visualising deformation in sandbox models (Almqvist and Koyi, 2018; Schöffisch et al., 2020, 2022).

385 In the models of this study, the magnetic fabric also reflects deformation and the development of structures. In addition, this study reveals an overprint of magnetic fabric due to inversion, specifically, differences are monitored between extensional to compressional tectonic environments. Extension did not result in penetrative strain in the models, which is indicated by a persistent initial fabric throughout the hanging wall (i.e., graben) and footwalls of Model I and the sharp change in degree of anisotropy between normal faults and in areas away from the faults. In contrast, in shortened models (e.g., Schöffisch et al., 390 2022) or inverted models (models II and III of this study), shortening leads to development of penetrative strain in areas away from the faults. Consequently, the magnetic fabric is sensitive to strain changes in compressional regimes, but further studies are required for depicting extensional fabrics in more details in sandbox models.

As the models simulate brittle behaviour of upper crustal rocks without taking into account processes like crystal-plastic deformation, fluid migration, and recrystallisation of magnetic contributors (i.e., changes in magnetic mineralogy and 395 development of sub-fabric), changes to the initial fabric in the models are solely related to grain reorientation. Such modelling setup and the combination of sandbox modelling with magnetic fabric analyses enables investigation, visualization, and highlighting the importance of grain reorientation in natural analogues.

### 5.2 Outlook: From limitations towards future models

400 As Eisenstadt and Sims (2005) and Deng et al. (2019) documented, there is no or very limited reactivation of pre-existing normal faults during inversion of such a model setup using loose sand above a ridged basal plate. In addition, an extensional fabric is not displayed in these models. Therefore, it may be necessary to prepare similar experiments simulating the development of a basin and its inversion with higher complexity. For example, testing syn-tectonic basin sedimentation to create magnetic lineation in basin fill, or using different materials (e.g., wet clay) to produce extensional structures (e.g., roll- 405 over anticlines; cf. Eisenstadt and Withjack, 1995; Eisenstadt and Sims, 2005). Moreover, different materials (Eisenstadt and Sims, 2005), oblique inversion (Dubois et al., 2002; Deng et al., 2019), or different modelling setups with viscous décollement (e.g., Roca et al, 2006; Del Ventisette et al., 2006 and references therein) lead to a reactivation of normal faults within the models. In such cases, investigating a magnetic fabric overprint due to fault reactivation is of great interest.





## 410 6 Conclusions

Three sandbox models were created to investigate the magnetic fabric in similar structures at different stages of basin inversion. Two distinct magnetic fabrics are observed in the extension model (Model I) prior to model inversion: an initial fabric away from the faults and normal fault-induced fabric. With subsequent inversion (i.e., models II and III), the magnetic fabric is overprinted by layer-parallel compaction (i.e., penetrative strain), developing a penetrative-strain-induced fabric.

415 During inversion of models II and III, thrusts formed with different stages of thrust maturity. This different thrust maturity is also reflected in the magnetic fabric and shows a different degree of alignment of the magnetic foliation parallel to the thrust surface. Although, normal faults and thrust faults showed a similar amount of displacement, their magnetic fabric differs from each other; thrusting is more efficient in aligning the magnetic fabric compared to normal faulting.

During inversion, the pre-existing normal faults define weak zones within a developing pop-up structure and deform during  
 420 inversion even though they show very little sign of inverted kinematics. This deformation is manifested by fault steepening that affects the magnetic fabric to become similar to a penetrative strain-induced fabric.

Irrespective of the orientation of principal axes, changes and gradients in the degree of anisotropy are identified depicting changes in deformation pattern in the models. In extended models (Model I), the magnetic fabrics from different parts of the model are distinct from each other. However, the magnetic fabric in the inverted models show an overprint from initial fabric  
 425 towards penetrative strain-induced fabric, which develops into a fault-induced fabric along the thrusts.

## Appendices

Additional figures with explanation for this study are summarized in the Supporting Information S1. S1 includes figures and  
 430 tables analysing the narrowing of the basin during inversion (Fig. S1 in S1) as well as an advanced analysis of the structure-to-sample-size ratio for AMS data at the faults (Fig. S2 in S1).

## Data availability

The AMS data from the three models of this study are published at the open-source online data repository hosted by Mendeley  
 435 Data (Schöfisch, 2022) with the following doi: 10.17632/bcxzzyrzj3.1 .

## Authors contribution

TS: conceptualization, methodology, formal analysis, interpretation, writing – original draft, writing – review & editing, visualization; HK & BA: interpretation, writing – review & editing, supervision, funding acquisition

440



## Competing interests

The authors declare no competing interests relevant to this study.

## 445 Acknowledgements

This study is supported by a research grant from the Swedish Research Council to HK and BA (VR, 2017–04519). Thanks are due to LKAB Minerals Luleå (Sweden) for providing the magnetite for modelling. Moreover, we thank the editors of this special issue for this opportunity.

## References

- 450 Almqvist, B.S.G. and Koyi, H.: Bulk strain in orogenic wedges based on insights from magnetic fabrics in sandbox models. *Geology* 46, 483–486. <https://doi.org/10.1130/G39998.1>, 2018.
- Averbuch, O., Frizon de Lamotte, D., and Kissel, C.: Magnetic fabric as a structural indicator of the deformation path within a fold-thrust structure: a test case from the Corbières (NE Pyrenees, France). *Journal of Structural Geology* 14, 461–474. [https://doi.org/10.1016/0191-8141\(92\)90106-7](https://doi.org/10.1016/0191-8141(92)90106-7), 1992.
- 455 Bakhtari, H.R., Frizon de Lamotte, D., Aubourg, C., and Hassanzadeh, J.: Magnetic fabrics of Tertiary sandstones from the Arc of Fars (Eastern Zagros, Iran). *Tectonophysics* 284, 299–316. [https://doi.org/10.1016/0040-1951\(97\)00179-0](https://doi.org/10.1016/0040-1951(97)00179-0), 1998.
- Bonini, M., Sani, F., and Antonielli, B.: Basin inversion and contractional reactivation of inherited normal faults: A review based on previous and new experimental models. *Tectonophysics* 522–523, 55–88. <https://doi.org/10.1016/j.tecto.2011.11.014>, 2012.
- 460 Borradaile, G.J.: Magnetic susceptibility, petrofabrics and strain. *Tectonophysics* 156, 1–20. [https://doi.org/10.1016/0040-1951\(88\)90279-X](https://doi.org/10.1016/0040-1951(88)90279-X), 1988.
- Borradaile, G. J.: Correlation of strain with anisotropy of magnetic susceptibility (AMS). *Pure and Applied Geophysics PAGEOPH*, 135(1), 15–29. <https://doi.org/10.1007/BF00877006>, 1991.
- Borradaile, G.J. and Henry, B.: Tectonic applications of magnetic susceptibility and its anisotropy. *Earth-Science Reviews* 42, 49–93. [https://doi.org/10.1016/S0012-8252\(96\)00044-X](https://doi.org/10.1016/S0012-8252(96)00044-X), 1997.
- 465 Borradaile, G.J. and Jackson, M.: Anisotropy of magnetic susceptibility (AMS); magnetic petrofabrics of deformed rocks *Geol. Soc. Spec. Publ.*, 238, pp. 299–360, 2004.
- Burmeister, K. C., Harrison, M. J., Marshak, S., Ferré, E. C., Bannister, R. A., and Kodama, K. P.: Comparison of Fry strain ellipse and AMS ellipsoid trends to tectonic fabric trends in very low-strain sandstone of the Appalachian fold-thrust belt. *Journal of Structural Geology*, 31(9), 1028–1038, 2009.
- 470 Burgin, H.B., Robion, P., and Amrouch, K.: Layer parallel stretching? Characterising magnetic and pore-fabric styles at a rifted continental margin: New insights from the Otway Ranges, Australia. *Tectonophysics* 815, 228975. <https://doi.org/10.1016/j.tecto.2021.228975>, 2021.
- 475 Cifelli, F., Mattei, M., Chadima, M., Hirt, A.M., and Hansen, A.: The origin of tectonic lineation in extensional basins: Combined neutron texture and magnetic analyses on “undeformed” clays. *Earth and Planetary Science Letters* 235, 62–78. <https://doi.org/10.1016/j.epsl.2005.02.042>, 2005.



- De Lamotte Frizon, D., Souque, C., Grelaud, S., and Robion, P.: Early record of tectonic magnetic fabric during inversion of a sedimentary basin - short review and examples from the Corbières transfer zone (France). *Bulletin de La Societe Geologique de France* 173, 461–469. <https://doi.org/10.2113/173.5.461>, 2002.
- 480 Del Ventisette, C., Montanari, D., Sani, F., and Bonini, M.: Basin inversion and fault reactivation in laboratory experiments. *Journal of Structural Geology* 28, 2067–2083. <https://doi.org/10.1016/j.jsg.2006.07.012>, 2006.
- Deng, H., Koyi, H.A., and Zhang, J.: Modelling oblique inversion of pre-existing grabens. *Geological Society Special Publication* 487, 263–290. <https://doi.org/10.1144/SP487.5>, 2019.
- Dubois, A., Odonne, F., Massonnat, G., Lebourg, T., and Fabre, R.: Analogue modelling of fault reactivation: tectonic inversion and oblique remobilisation of grabens, *J. Struct. Geol.*, 24, 1741–1752, [https://doi.org/10.1016/S0191-8141\(01\)00129-8](https://doi.org/10.1016/S0191-8141(01)00129-8), 2002.
- 485 Eisenstadt, G. and Withjack, M.O.: Estimating inversion: Results from clay models. *Geological Society Special Publication* 88, 119–136. <https://doi.org/10.1144/GSL.SP.1995.088.01.08>, 1995.
- Eisenstadt, G. and Sims, D.: Evaluating sand and clay models: Do rheological differences matter? *Journal of Structural Geology* 27, 1399–1412. <https://doi.org/10.1016/j.jsg.2005.04.010>, 2005.
- 490 García-Lasanta, C., Oliva-Urcia, B., Román-Berdiel, T., Casas, A.M., and Hirt, A.M.: Understanding the Mesozoic kinematic evolution in the Cameros basin (Iberian Range, NE Spain) from magnetic subfabrics and mesostructures. *Journal of Structural Geology*, 66: 84–101. <https://doi.org/10.1016/j.jsg.2014.05.013>, 2014.
- García-Lasanta, C., Oliva-Urcia, B., Román-Berdiel, T., Casas, A.M., Gil-Peña, I., Sánchez-Moya, Y., Sopeña, A., Hirt, A.M., and Mattei, M.: Evidence for the Permo-Triassic transtensional rift in the Iberian Range (NE Spain) according to magnetic fabrics results. *Tectonophysics* 651–652: 216–231. <https://doi.org/10.1016/j.tecto.2015.03.023>, 2015.
- 495 García-Lasanta, C., Oliva-Urcia, B., Casas-Sainz, A.M., Román-Berdiel, T., Izquierdo-Llavall, E., Soto, R., Calvin, P., Moussaid, B., El Ouardi, H., Kullberg, J.C., and Villalain, J.J.: Inversion tectonics and magnetic fabrics in Mesozoic basins of the Western Tethys: A review. *Tectonophysics* 745, 1–23. <https://doi.org/10.1016/j.tecto.2018.08.005>, 2018.
- Hirt, A.M., Lowrie, W., Clendenen, W.S., and Kligfield, R.: The correlation of magnetic anisotropy with strain in the Chelmsford Formation of the Sudbury Basin, Ontario. *Tectonophysics* 145, 177–189. [https://doi.org/10.1016/0040-1951\(88\)90194-1](https://doi.org/10.1016/0040-1951(88)90194-1), 1988.
- 500 Hrouda, F. and Janák, F.: The changes in shape of the magnetic susceptibility ellipsoid during progressive metamorphism and deformation. *Tectonophysics* 34, 135–148. [https://doi.org/10.1016/0040-1951\(76\)90181-5](https://doi.org/10.1016/0040-1951(76)90181-5), 1976.
- Hrouda, F.: Magnetic anisotropy of rocks and its application in geology and geophysics. *Geophysical Surveys*, 5(1), 37–82. <https://doi.org/10.1007/BF01450244>, 1982.
- Jelinek, V.: Characterization of the magnetic fabric of rocks. *Tectonophysics* 79, T63–T67. [https://doi.org/10.1016/0040-1951\(81\)90110-4](https://doi.org/10.1016/0040-1951(81)90110-4), 1981.
- 505 Kligfield, R., Owens, W.H., Lowrie, W.: Magnetic susceptibility anisotropy, strain, and progressive deformation in Permian sediments from the Maritime Alps (France). *Earth and Planetary Science Letters* 55, 181–189. [https://doi.org/10.1016/0012-821X\(81\)90097-2](https://doi.org/10.1016/0012-821X(81)90097-2), 1981.
- Koyi, H.: Mode of internal deformation in sand wedges. *Journal of Structural Geology* 17, 293–300. [https://doi.org/10.1016/0191-8141\(94\)00050-A](https://doi.org/10.1016/0191-8141(94)00050-A), 1995.
- 510



- Koyi, H.A., Sans, M., Teixell, A., and Zeyen, H.: The Significance of Penetrative Strain in the Restoration of Shortened Layers-Insights from Sand Models and the Spanish Pyrenees. *Thrust Tectonics and Hydrocarbon Systems: AAPG Memoir*. 82, 1–16, 2003.
- Marcén, M., Román-Berdiel, T., Casas-Sainz, A.M., Soto, R., Oliva-Urcia, B., and Castro, J.: Strain variations in a seismogenic normal fault (Baza Sub-basin, Betic Chain): Insights from magnetic fabrics (AMS). *Tectonophysics* 765, 64–82. <https://doi.org/10.1016/j.tecto.2019.05.014>, 2019.
- 515 Mattei, M., Sagnotti, L., Faccenna, C., and Funicello, R.: Magnetic fabric of weakly deformed clay-rich sediments in the extensional tectonics. *Tectonophysics* 271, 107–122, 1997.
- Mattei, M., Speranza, F., Argentieri, A., Rossetti, F., Sagnotti, L., and Funicello, R.: Extensional tectonics in the Amantea basin (Calabria, Italy): A comparison between structural and magnetic anisotropy data. *Tectonophysics* 307, 33–49. [https://doi.org/10.1016/S0040-1951\(99\)00117-1](https://doi.org/10.1016/S0040-1951(99)00117-1), 1999.
- 520 Mulugeta, G. and Koyi, H.: Episodic accretion and strain partitioning in a model sand wedge. *Tectonophysics* 202, 319–333. [https://doi.org/10.1016/0040-1951\(92\)90117-O](https://doi.org/10.1016/0040-1951(92)90117-O), 1992.
- Oliva-Urcia, B., Casas, A.M., Soto, R., Villalaín, J.J., and Kodama, K.: A transtensional basin model for the Organyà basin (central southern Pyrenees) based on magnetic fabric and brittle structures. *Geophysical Journal International*, 184 (1): 111–130. <https://doi.org/10.1111/j.1365-246X.2010.04865.x>, 2010.
- 525 Oliva-Urcia, B., Román-Berdiel, T., Casas, A.M., Bogalo, M.F., Osácar, M.C., and García-Lasanta, C.: Transition from extensional to compressional magnetic fabrics in the cretaceous Cabuérniga basin (North Spain). *Journal of Structural Geology*, 46: 220–234. <https://doi.org/10.1016/j.jsg.2012.09.001>, 2013.
- Oliva-Urcia, B., Casas, A.M., Moussaid, B., Villalaín, J.J., El Ouardi, H., Soto, R., Torres-López, S., and Román-Berdiel, T.: Tectonic fabrics vs. mineralogical artifacts in AMS analysis: a case study of the Western Morocco extensional Triassic basins. *Journal of Geodynamics*, 94–95: 13–33. <https://doi.org/10.1016/j.jog.2016.01.004>, 2016.
- 530 Parés, J.M., Van der Pluijm, B.A., and Dinarès-Turell, J.: Evolution of magnetic fabrics during incipient deformation of mudrocks (Pyrenees, northern Spain). *Tectonophysics* 307, 1–14. [https://doi.org/10.1016/S0040-1951\(99\)00115-8](https://doi.org/10.1016/S0040-1951(99)00115-8), 1999.
- Parés, J.M., and Van Der Pluijm, B.A.: Evaluating magnetic lineations (AMS) in deformed rocks. *Tectonophysics* 350, 283–298. [https://doi.org/10.1016/S0040-1951\(02\)00119-1](https://doi.org/10.1016/S0040-1951(02)00119-1), 2002.
- 535 Parés, J.M.: Sixty years of anisotropy of magnetic susceptibility in deformed sedimentary rocks. *Frontiers in Earth Science* 3, 4. <https://doi.org/10.3389/feart.2015.00004>, 2015.
- Roca, E., Sans, M., and Koyi, H.A.: Polyphase deformation of diapiric areas in models and in the eastern Prebetics (Spain). *AAPG Bulletin*, 90, 115–136. <https://doi.org/10.1306/07260504096>, 2006.
- 540 Sagnotti, L., Faccenna, C., Funicello, R., and Mattei, M.: Magnetic fabric and structural setting of Plio-Pleistocene clayey units in an extensional regime: the Tyrrhenian margin of central Italy. *Journal of Structural Geology* 16, 1243–1257. [https://doi.org/10.1016/0191-8141\(94\)90067-1](https://doi.org/10.1016/0191-8141(94)90067-1), 1994.
- Schöfisch, T., Koyi, H., and Almqvist, B.: Influence of décollement friction on anisotropy of magnetic susceptibility in a fold-and-thrust belt model. *Journal of Structural Geology* 144. <https://doi.org/10.1016/j.jsg.2020.104274>, 2020.
- 545 Schöfisch, T., Koyi, H., and Almqvist, B.: Magnetic Fabric Signature Within a Thrust Imbricate; an Analog Modeling Approach. *Tectonics* 41, 1–18. <https://doi.org/10.1029/2021TC007054>, 2022.



- Schöfisch, T.: “Magnetic Fabric Distribution in inverted Basin Sandbox Models”, Mendeley Data, V1, doi: 10.17632/bexzzyrzj3.1, 2022
- Soto, R., Casas-Sainz, A.M., Villalaín, J.J., and Oliva-Urcia, B.: Mesozoic extension in the Basque-Cantabrian basin (N Spain). Contributions from AMS and brittle mesostructures. *Tectonophysics*, 445: 373-394. <https://doi.org/10.1016/j.tecto.2007.09.007>, 2007
- Soto, R., Casas-Sainz, A.M., Villalaín, J.J., Gil-Imaz, A., Fernández-González, G., Del Río, P., Calvo, M., and Mochales, T.: Characterizing the Mesozoic extension direction in the northern Iberian plate margin by anisotropy of magnetic susceptibility (AMS). *Journal of the Geological Society*, 165: 1007-1018. <https://doi.org/10.1144/0016-76492007-163>, 2008.
- Soto, R., Kullberg, J.C., Oliva-Urcia, B., Casas-Sainz, A.M., and Villalaín, J.J.: Switch of Mesozoic extensional tectonic style in the Lusitanian basin (Portugal): Insights from magnetic fabrics. *Tectonophysics*, 536-537: 122-135. <https://doi.org/10.1016/j.tecto.2012.03.010>, 2012.
- Soto, R., Larrasoña, J.C., Beamud, E., and Garcés, M.: Early-Middle Miocene subtle compressional deformation in the Ebro foreland basin (northern Spain); insights from magnetic fabrics. *Comptes Rendus Geoscience*, 348(3-4): 213-223. <https://doi.org/10.1016/j.crte.2015.10.009>, 2016.
- Tong, H., Koyi, H., Huang, S., and Zhao, H.: The effect of multiple pre-existing weaknesses on formation and evolution of faults in extended sandbox models. *Tectonophysics* 626, 197–212. <https://doi.org/10.1016/j.tecto.2014.04.046>, 2014.